Research Article | Vol. 31, No. 25 / 4 Dec 2023 / Optics Express 42687
Optics EXPRESS

Half-broadband two-dimensional electronic spectroscopy with active noise reduction

GIOVANNI BRESSAN,[1] ISMAEL A. HEISLER,[2] GREGORY M. GREETHAM,[3] AMY EDMEADES,[3] AND STEPHEN R. MEECH[1,*]

[1]School of Chemistry, Norwich Research Park, University of East Anglia, Norwich NR4 7TJ, UK
[2]Instituto de Física, Universidade Federal do Rio Grande do Sul - UFRGS, Avenida Bento Gonçalves, 9500, Porto Alegre, Brazil
[3]Central Laser Facility, Rutherford Appleton Laboratory, Didcot, OX11 0QX, UK
*s.meech@uea.ac.uk

Abstract: Two-dimensional electronic spectroscopy (2DES) provides detailed insight into coherent ultrafast molecular dynamics in the condensed phase. Here we report a referenced broadband pump-compressed continuum probe half-broadband (HB) 2DES spectrometer in a partially collinear geometry. To optimize signal-to-noise ratio (SNR) we implement active noise reduction referencing, which has not previously been applied in 2DES. The method is calibrated against the well characterized 2DES response of the oxazine dye cresyl violet and demonstrated at visible wavelengths on the photochromic photoswitch 1,2-Bis(2-methyl-5-phenyl-3-thienyl) perfluorocyclopentene (DAE). The SNR is improved by a factor of ~2 through active referencing. This is illustrated in an application to resolve a low frequency mode in the excited electronic state of DAE, yielding new data on the reaction coordinate. We show that the active noise reduction referencing, coupled with the rapid data collection, allows the extraction of weak vibronic features, most notably a low frequency mode in the excited electronic state of DAE.

1. Introduction

Technological advances in ultrafast science over the past two decades enabled time-domain interferometry at infrared and optical frequencies [1,2]. Two-dimensional electronic spectroscopy (2DES) is a four-wave mixing technique in which, for a fixed population (waiting) time (T, corresponding to the pump-probe delay in transient absorption, TA), a coherence time delay (τ) between two replicas of a pump pulse, is scanned with interferometric precision. In this method the detection axis is directly measured by spectrally dispersing the probe and the excitation axis is obtained by a Fourier transform over τ. The resulting 2D spectrum can be thought of as an excitation frequency resolved TA spectrum measured at T. Stretching TA data along this additional frequency axis has numerous advantages: congested steady-state electronic spectra, such as in naturally occurring and artificial coupled multi-chromophore systems, are better resolved; homogenous and inhomogeneous dephasing dynamics are separately determined; [2] vibronic coherence maps providing detailed insight into electronic-vibrational couplings are recovered [3,4]. Thus, 2DES has been extensively applied to investigate energy and charge transfer in photosynthetic complexes, [4–7] exciton coupling in dimers [8–11] and oligomers [12–14], analysis of vibronic coupling [15–17], nanostructured photonic materials [18,19] and fast photochemical reactions [20].

2DES poses several experimental challenges, especially the interferometric nature of the measurement, which makes it sensitive to phase fluctuations. Hence, early experimental developments focused on the generation of passively phase-stabilized pulse sequences. These relied on tuneable noncollinear optical parametric amplifier (NOPA) sources, combined with

#500017 https://doi.org/10.1364/OE.500017
Journal © 2023 Received 13 Jul 2023; revised 18 Sep 2023; accepted 11 Oct 2023; published 1 Dec 2023

Optics EXPRESS

diffractive optics, beamsplitters or combinations thereof, in a fully-noncollinear "BOXCARS" geometry. In this geometry, four degenerate replicas of a pulse excite and interrogate the sample at different times, and heterodyne the third-order signal (Fig. 1(a)) [21–26]. Precise control of the signal to local oscillator intensity ratio and background-free detection yield high signal-to-noise ratios (SNRs) [27,28]. While these methods allow full polarization control, [29,30] they are restricted to transitions which fall within the NOPA bandwidth, which is typically less than 3000 cm^{-1} (baseline-to-baseline). This is inadequate for the characterisation of the coherent dynamics in many systems of interest including many molecular energy, electron or proton transfer reactions for example [10,31,32].

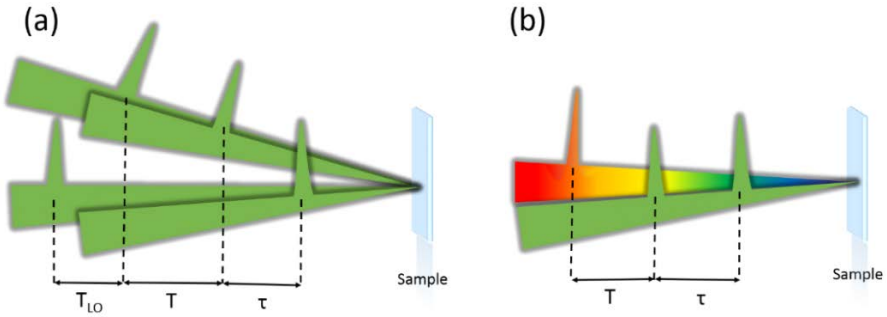

Fig. 1. Scheme of the pulse sequence and time delays for two dimensional electronic spectroscopy in: (a) fully-noncollinear degenerate "BOXCARS" and (b) pump-probe half-broadband geometries, in which green and rainbow represents NOPA and white-light beams, respectively. τ, T, and T_{LO} indicate coherence, waiting (population) and local oscillator times, respectively. T_{LO} is not shown in (b) as 2DES in pump-probe geometry is self-heterodyned.

This bandwidth limitation can be alleviated in BOXCARS 2DES by employing compressed nonlinearly broadened sources in place of NOPAs, such as hollow-core fibres (HCF) [33,34,35]. HCFs employed in a BOXCARS geometry can more than double the available bandwidth while retaining the advantages of background-free detection. However, HCF sources still have limited spectral coverage compared to the white-light continuum (WLC) probe employed in TA. This has led to efforts to utilize WLC in 2DES [36,37,38]. In either case full broadband measurements impose an additional layer of complexity on the 2DES experiment.

An alternative 'half broadband approach' has been developed [39–41]. Intrinsically phase-stable pulse pairs are available from pulse shapers such as acousto-optic programmable dispersive filters (AOPDF) or spatial light modulators (SLM). The combination of such pulse pairs as the "pump" with a WLC probe in a partially collinear "pump-probe" geometry allows measurement of 2DES for which the excitation axis has the NOPA bandwidth but the detection has the full WLC bandwidth exceeding ten thousand wavenumbers in the visible-NIR [41,42]. The geometry of such an experiment is a simple variation on the established TA layout and is sketched in Fig. 1(b). Significantly, pulse shapers, combined with phase-cycling algorithms, enable the retrieval of the real and imaginary parts of rephasing and nonrephasing responses and thus the absorptive $\chi^{(3)}$ without recourse to the projection-slice theorem [43,44]. Thus, the partially collinear, pump-probe geometry is an attractive route to 2DES. However, the method is a self-heterodyned measurement and thus suffers from an intrinsically lower SNR compared to background-free methods, as independent control of signal and local oscillator intensities is not possible. Fuller *et al.* [40] proposed a hybrid approach to improve SNR in HB 2DES, combining the advantages of pulse shaping and background-free geometries, at the price of measuring non-automatically phased data.

Optics EXPRESS

Here, we present a referenced HB 2DES spectrometer employing a NOPA pump pair obtained with shot-to-shot AOPDF pulse shaping, and a compressed WLC probe. Referencing, which is already a feature of many TA spectrometers, is complemented by use of an active noise reduction algorithm developed by Feng *et al.* [45] for heterodyned laser spectroscopies. The potential of this algorithm has been addressed in a few works, showing substantial SNR improvement in time-resolved spectroscopy [46,47]. To the best of our knowledge, the present work is the first to demonstrate referenced active noise reduction in 2DES. As an example of the method we investigate 2DES in a dilute diarylarene photochromic photoswitch with the previously well characterized 2DES of cresyl violet as a control.

2. Methods

2.1. Half-broadband two-dimensional electronic spectrometer layout

The layout of our spectrometer is based on our earlier fs transient absorption experiment [38,48,49] and is similar to those described elsewhere [19,39,41] (Fig. 2). A commercial noncollinear optical parametric amplifier (NOPA, Topas White, Light Conversion) provides the pump pulse pair of pulsewidth 25-30 fs (corresponding to ~1500 cm^{-1} bandwidth) tuneable from 20400 to 13200 cm^{-1}. It is pumped by a regenerative amplifier operating at 800 nm and 1 kHz (Spitfire Ace, Spectra-Physics). The NOPA beam is routed to an AOPDF (Dazzler, Fastlite) synchronized to the regenerative amplifier. The AOPDF generates a collinear phase-locked pulse pair with adjustable coherence time delay τ (see inset of Fig. 2) and relative carrier wave phase shift φ_{1-2}, i.e., the phase difference between the first and the second pump pulses [43,44]. The details of the data acquisition and processing are given below. After the shaping stage, a commercial "grism" compressor (Fastlite) (GC) compensates for the dispersion introduced by the AOPDF and the other transmissive optics in the NOPA beam path [50].

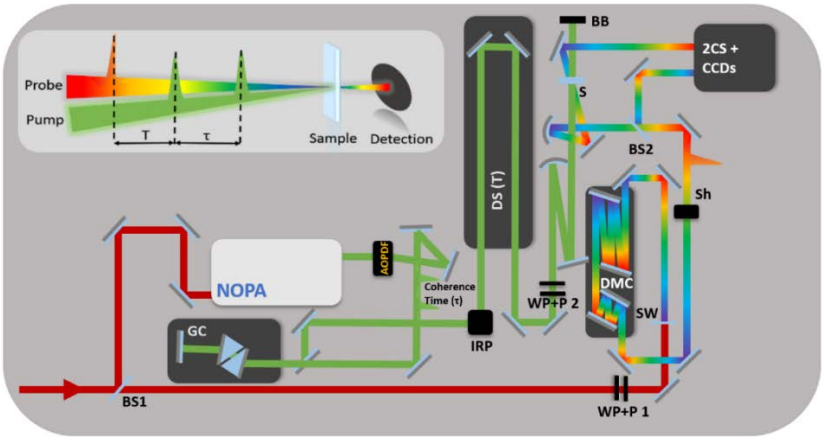

Fig. 2. Half-broadband two-dimensional electronic spectroscopy (HB2DES) experimental setup where: BS1,2 beamsplitters; NOPA noncollinear optical parametric amplifier; AOPDF acousto-optic programmable dispersive filter (Dazzler, Fastlite); GC folded grism compressor; IRP image rotating periscope; DS(T) mechanical delay stage; WP+P1, 2 half-wave plates and polarizers combination; SW sapphire window; DMC dispersive mirrors compressor; Sh shutter; S sample; BB beam block; 2CS+CCDs dual channel prism-based spectrometer and full-frame transfer charge coupled device detectors. The upper left corner inset illustrates the pulse arrival sequence on the sample as well as the time delays between pulses.

After the compression stage, the pump pulse pair is routed, *via* an image rotating periscope (setting *s*-polarisation again) to a retroreflector mounted on a linear translation stage (Physik

Optics EXPRESS

Instrumente) which introduces the waiting (population) time delay (T) between the second pump and the WLC probe pulse (see inset of Fig. 2). The WLC probe is generated by focusing <1% of the 800 nm amplifier output, into a static 3 mm sapphire window. The pump pair goes through a half-wave plate and polarizer, which sets them at the magic angle with respect to the probe and is focused onto the sample by a concave mirror to a spot of 160 µm at sample position.

The WLC spans 415-800 nm (24000-12500 cm^{-1}) and is group dispersion delay-corrected by a double-angle dispersive mirrors compressor. The resulting instrument response function (IRF) is flat across the whole probe spectrum and <50 fs, as determined by spectrally-resolving the instantaneous Kerr response between compressed NOPA and WLC in a 1 mm cell filled with neat cyclohexane, see Supplement 1, Fig. S1. After recompression, the WLC travels through an optical shutter (Sh, Thorlabs SH05) synchronized to the AOPDF and is divided by a 50:50 beamsplitter into a signal and a reference beam. The signal beam is focused onto the sample to a 40 µm diameter spot, at a ~4°crossing angle with the pumps. The reference beam does not pass through the sample. After the sample, the self-heterodyned signal is recollimated, and signal and reference are routed to a home-built dual channel prism spectrometer and imaged onto a pair of 16-bit A/D full frame transfer CCD detectors (1024 pixels, Entwicklungsbüro Stresing) synchronized to the AOPDF and read out at 1 kHz, with an integration time of 200 µs.

2.2. Data acquisition and processing

The AOPDF is programmed to scan the coherence time in 120 evenly spaced delay points between -95 fs and 0 fs ($\Delta\tau$= 0.7917 fs), corresponding to a non-rotating frame Nyquist wavelength of 450 nm (22000 cm^{-1}), well above the short wavelength cut-off of the NOPA at 20400 cm^{-1}). In BOXCARS 2DES setups scanning positive or negative times yields rephasing or nonrephasing signals, respectively [51]. In contrast, the pump-probe geometry causes the rephasing and nonrephasing signals to be emitted along the same direction [52,53,28] such that $\boldsymbol{k}_3$, is self-heterodyned by the collinear probe beam. Here, the only advantage of scanning negative rather than positive coherence times in pump-probe 2DES is to enable independent control of the coherence and the population time delays. Time zero is defined as the coincidence between the pump pair and the continuum probe pulses. Whilst $\tau = 0$ fs is unambiguously defined by the AOPDF, $T = 0$ fs is obtained by evaluating the maximum of the IRF, as shown in Fig. S1.

The φ_{1-2} dependent 2DES response is then isolated from the φ_{1-2}-independent signals (linear absorption, TA and scattering from each pump pulse), according to a three-frame phase cycling procedure [43,44]. For each value of τ, φ_{1-2} is cycled through 0, $2\pi/3$ and $4\pi/3$ in three consecutive laser shots, which yields the highest SNR [33,54]. To minimize sample exposure, the AOPDF is programmed to block the NOPA beam during data transfer, processing and mechanical delay stage motion.

The real and imaginary parts of rephasing and nonrephasing signals are then acquired using a collection and averaging procedure described in Supplement 1. The phase-cycled averaged data are inverse Fourier-transformed over the detection frequency, obtaining 2D data as a function of the signal time t. These are multiplied by a Heaviside function to impose causality, then Fourier transformed over t to retrieve the detection frequency dimension. Finally, the Fourier transform over τ of the causality-imposed data yields real and imaginary parts of rephasing and nonrephasing data for a given T, and their sum yields the absorptive spectra [44,55]. The acquisition sequence and data processing times are summarized in Figs. S2-3. The process described is repeated for each population time T.

The phase cycling procedure does not entirely remove pump scattering. To correct this, a shutter blocks the probe beam during the acquisition of the first burst of shots ($N = 0$, where N is the number of CCD bursts over which each waiting time is averaged) at each value of T; the process has been described by Fuller [40]. This allows isolation of the direct scattering signal, yielding a baseline that is updated every 15-60 s, which is then subtracted from the following

Optics EXPRESS

N-1 iterations. These data are then used as benchmark for the calibration of the excitation and detection frequency axes, as the interferometric signal between light scattered off the pump pair has to be centred on the diagonal of the 2D spectrum [56].

2.3. Referencing and active noise reduction

Here we applied and tested the active noise reduction algorithm of Feng *et al.* [45] to HB2DES. This method has been successfully applied to femto- and nanosecond transient mid-infrared spectroscopy, 2DIR and visible transient absorption showing remarkable improvement of the SNR [46,47].

In self-heterodyned TA measurements signal and reference are simultaneously measured on a pair of matched CCD detectors. Noise caused by fluctuations of the probe intensity is removed by computing the difference (or the ratio, if in ΔOD [37]) between signal and reference spectra. Such spectrally resolved ratiometric referencing has not been applied, to the best of our knowledge, to 2DES in either BOXCARS or pump-probe geometries, and may not be easily implemented, although Bizimana *et al.* introduced an "integrated" balanced detection scheme for 2DES in which the local oscillator is referenced against a photodiode [57]. These referencing methods rely on the assumptions of signal and reference detectors having identical noise floors (dark/electronic noise) and alignment. More formally, following Robben *et al.*, [47] the total noise (n) of each channel can be expressed:

$$n_S = n_S^{WLC} + n_S^f \tag{1a}$$

$$n_R = n_R^{WLC} + n_R^f \tag{1b}$$

where S and R subscripts indicate noise of the signal and reference channels, respectively, and the total noise is the sum of that due to WLC fluctuations, indicated by the *WLC* superscript and a detector noise floor, indicated by the f superscript.

The total measured signal S will thus be:

$$S = S_{real} + n_S \tag{2}$$

where S_{real} is the ideal, noiseless, signal for a given pair of τ, T delays. If the signal and reference CCDs were identical and their alignment was perfectly matched, $n_S^{WLC} = n_R^{WLC}$, and subtracting 1b from 2 yields a noise corrected spectrum S_{corr}:

$$S_{corr} = S_{real} + n_S^f - n_R^f \tag{3}$$

Although, as n_S^f and n_R^f are uncorrelated variables, this referencing method will add, in a root-sum-square way, [47] the floor noise of the reference channel to the signal. Furthermore, exactly matched CCDs and identical alignment are difficult to achieve, i.e., $n_S \neq n_R$.

The active noise reduction algorithm proposed by Feng *et al.* [45] provides a simple method to address the noise floor and alignment mismatch issues. Their method relies on the calibration of a correlation matrix $\mathbf{B}$ (of sizes $N_S \times N_R$, where $N_{S,R}$ is the number of pixels of the signal and reference detectors), mapping the reference channel noise onto the signal channel so that:

$$n_S \cong \boldsymbol{B} \cdot n_R \tag{4}$$

And the corrected signal S_{corr}:

$$S_{corr} = S - \boldsymbol{B} \cdot n_R \tag{5}$$

n_R in Eq. (5) is the three-frame phase-cycled reference channel noise matrix, whose dimensions are $1 \times N_R$. For processing speed reasons, we employed $N_R = 150$ pixels, chosen in the region where the continuum shows more spectral modulations and instability (13000-16000 cm^{-1}); other

Optics EXPRESS

regions of the reference channel were tried and gave similar or less good performance. The coefficients of the noise mapping matrix **B** are estimated by least-squares minimisation of the mean residual noise, defined as:

$$\Delta n = |n_S - \boldsymbol{B} \cdot n_R| \tag{6}$$

where the noise of the signal channel n_S is determined by collecting, and phase-cycling, a burst of "blank" probe shots, obtained by shutting the pump beam, and thus enforcing $S_{real} = 0$, in agreement with Eq. (2).

Least-squares minimisation of Eq. (6) yields:

$$\boldsymbol{B} = \langle n_S \cdot {n_R}^T \rangle \cdot \langle n_R \cdot {n_R}^T \rangle^{-1} \tag{7}$$

where angled brackets denote averaging and T superscripts indicate transposed matrices. The number of shots for the calibration of the $\boldsymbol{B}$ matrix (1080) was chosen according to Robben *et al.* suggesting that the noise reduction performance of the algorithm reaches a plateau for a number of shots approximating 10x the reference number of pixels N_R [47]. Increasing the number of calibration shots allows an increase in the size of N_R, yielding, in principle, a better SNR. However, the trade-off would be a nonlinear increase in processing time between the acquisitions of consecutive 2D spectra.

3. Results and discussion

For the purpose of calibration of the HB2DES spectrometer we measured the real and imaginary parts of rephasing, nonrephasing and absorptive 2D spectra of the widely studied oxazine dye cresyl violet perchlorate (CV) in ethanol (EtOH). Our data are in very good agreement with literature 2DES of CV obtained with the BOXCARS method; [34,51,58,59,60,61] CV data at $T = 200$ fs are reported in Supplement 1 (Figs. S4-6). Figure S7 shows the single trace time-domain rephasing real residuals and their Fourier transform, where the very well characterized oxazine core ground state vibration at 588 cm^{-1} is evident (previously reported at 585 cm^{-1} by Ma *et al.* [34] and at 589 cm^{-1} by Lu *et al.* [59]).

To demonstrate the advantages of active noise reduction, the setup is benchmarked by acquiring HB2DES of 1,2-Bis(2-methyl-5-phenyl-3-thienyl) perfluorocyclopentene (DAE). DAE is a photoswitching diarylethene derivative, which is known to undergo an ultrafast ring opening reaction following electronic excitation in the visible region of the spectrum. 2DES has the potential to provide new insights into this reaction, and especially to resolve any role for vibrational coherences in directing motion along the reaction coordinate. This presents a greater challenge to HB2DES than CV as its transition dipole moment is five times weaker, with correspondingly weaker nonlinear signals. [62] The molecular structure of the closed form of DAE is shown in the upper right corner of Fig. 3(a), where steady-state absorption and emission spectra ($\lambda_{exc} = 565$ nm) in cyclohexane (CHX) are reported. A 600 mOD solution (1 mm cell) of the closed form of DAE in CHX was obtained by continuous irradiation of the UV absorbing open form with a 285 nm LED (Thorlabs), at 5 mW for 2 hours. HB2DES spectra were collected without flowing as no differences in the absorption spectrum before and after the measurement were observed, consistent with the low quantum yield of ring opening [63,64]. The sample was excited by pulses centred at 16900 cm^{-1} with ~0.8 μJ energy per pulse pair and probed by the WLC spanning 13000-24000 cm^{-1}. Population times were scanned between 0 and 1200 fs, in 10 fs steps. Absorptive HB2DES at $T = 300$ fs are reported in Fig. 3(b)-(d). The measurement was repeated either excluding (3b) or including (3c) the active noise reduction method described above. Uncorrected (raw) and noise corrected data averaged over 45 and 180 shots are shown in Supplement 1 (Figs. S8-9).

HB2DES spectra of DAE in CHX at $T = 300$ fs show a component arising from ground-state bleach (GSB) convoluted with stimulated emission (SE) between $\tilde{\nu}_3$ = 15000-19000 cm^{-1} and an

Optics EXPRESS

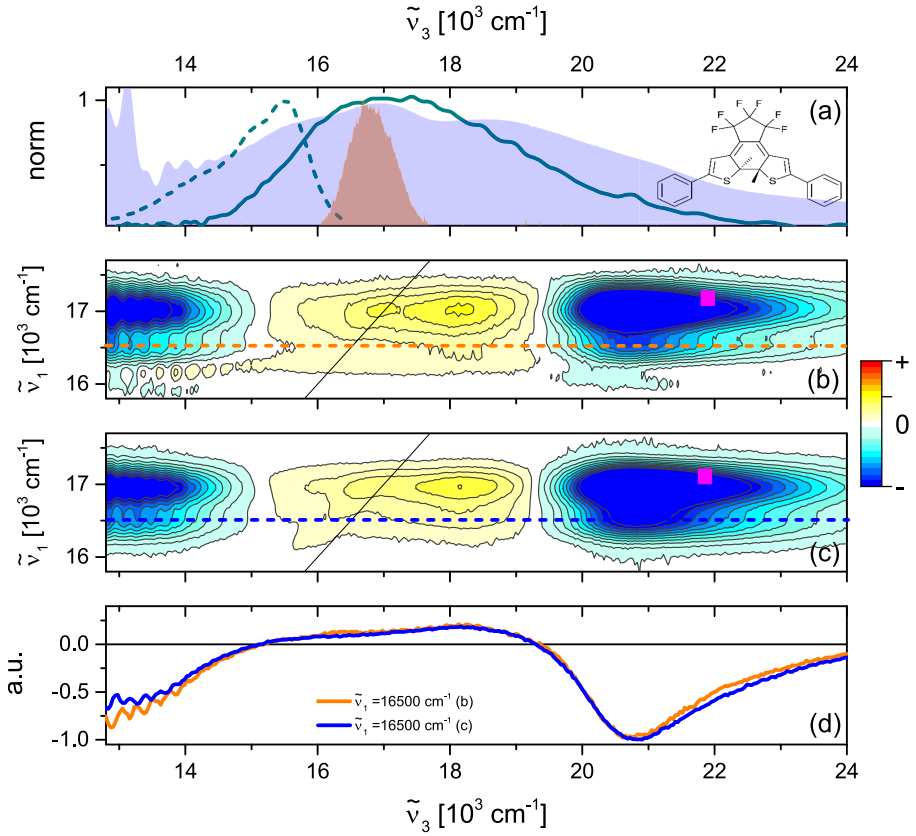

Fig. 3. (a) Normalized steady-state absorption (solid) and emission (dashed) of the photostationary state of DAE in cyclohexane, whose molecular structure is shown in the upper right corner. Normalized NOPA pump and probe spectra used for the HB 2DES measurements are shown as shaded orange and blue areas, respectively. (b) Real part of the absorptive 2D spectra of DAE at T=300 fs without noise and pump scattering corrections, each coherence time is averaged over 90 laser shots. The intensity is given by 21 evenly spaced contour lines, positive signals are shown in yellow and negative signals are shown in blue. (c) Same as (b), with noise and pump scattering corrections. (d) Slices of (b), (c), normalized at $\tilde{\nu}_3 = 20900\,\mathrm{cm}^{-1}$, taken at the positions marked by horizontal blue and orange dashed lines in (b), (c). The magenta squares mark specific positions that will be discussed below. The strong negative signals are saturated to highlight the differences between the low amplitude regions of the raw and referenced 2DES spectra.

excited state absorption contributions (ESA) extending from the near-infrared to the ultraviolet, with a peak at $\tilde{\nu}_3 = 20900\,\mathrm{cm}^{-1}$. Whilst 2DES was applied to the reaction dynamics of a merocyanine-spiropyran photoswitch by Kullmann *et al.* [20], 2DES of DAE has not been reported before.

Figure 3(b)-(c) show how the noise correction improves the SNR of the low-amplitude regions of the 2D spectra ($\tilde{\nu}_1$ = 15800-16500 cm^{-1}) and corrects some artefacts. In particular, the phase modulations, introduced by the dispersive mirror compressor (as in Supplement 1 of [65]) (Fig. 3(b)), which are particularly evident in the low amplitude edge of the ESA between $\tilde{\nu}_3$ = 12800-16000 cm^{-1}, are effectively suppressed by active noise reduction.

Figure 3(d) shows slices of the 2D spectra at excitation frequency $\tilde{\nu}_1 = 16500\,\mathrm{cm}^{-1}$, marked by horizontal orange (3b) and blue (3c) dashed lines. As expected these slices agree well with

Optics EXPRESS

previous TA spectra of DAE [66,67]. Again, the slice of the uncorrected 2D spectrum (orange) contains oscillatory artefacts on its low-energy side between 12800 and 15500 cm^{-1}. These features are partially suppressed by the use of the active noise reduction algorithm, as shown by the blue "slice". The noise floor of the experiment was measured by acquiring raw and noise corrected 2DES spectra at a negative waiting time (T = - 1500 fs). The results, shown in Figs. S 10-12 for 45, 90 and 180 shots averaging, show how the baseline modulations present in the raw spectra are successfully removed by the noise correction procedure. The SNR of the 2D spectra is quantitatively characterized by computing the inverse of the standard deviation $\sigma(\tau, \tilde{\nu}_3)$ of the interferogram acquired during the coherence time, at $\tilde{\nu}_3 = 13500\,cm^{-1}$, for τ values large enough that the signal has dephased, a procedure previously adopted by Kearns *et al.* [54]. These interferograms, extracted from figures Fig. 3(b), (c), are shown in Fig. 4 and show an increase of ~2.1 in $\sigma(\tau, \tilde{\nu}_3)^{-1}$ between unreferenced and referenced active noise corrected HB2DES. Figures S13-14 show the interferograms of the raw and noise corrected data obtained by averaging each coherence time over 45 or 180 shots. The measured SNR improvements are ~1.7 and ~2.2, respectively, showing how the enhancement due to the active noise correction does not vary significantly for this degree of averaging. The SNR enhancement due to the active noise reduction adds to the square root SNR improvement due to each 2D spectrum being averaged over more shots.

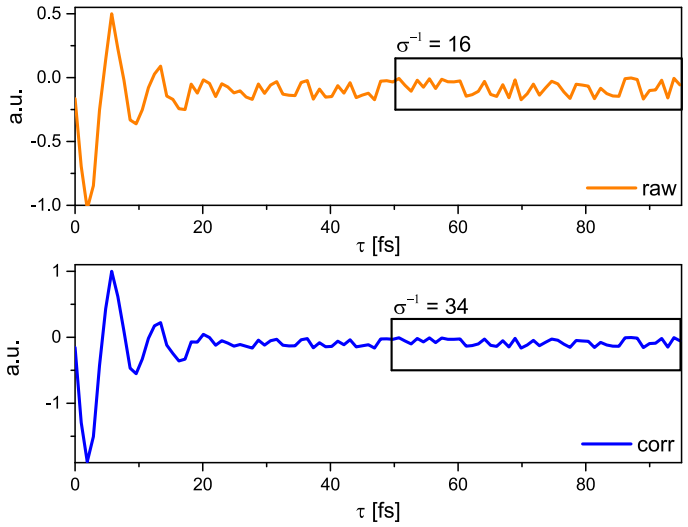

Fig. 4. Normalized absorptive real referenced and noise-corrected (blue) and unreferenced (orange) coherence time traces of DAE at a probe wavenumber of 13500 cm^{-1} and at T = 300 fs when each coherence time is averaged over 90 laser shots (taken from Figures 3(b) and (c)). The standard deviation σ was calculated over the points enclosed in the black rectangles and its inverse is proportional to the SNR. The ratio between the inverse standard deviations 34/16 ~ 2.13 which is the signal to noise improvement factor due to the active noise correction referencing scheme.

An important tool in the analysis of 2DES data is the extraction of "beatmaps". These report on modulations of the intensity, induced by coherently exciting ground or excited state Raman active modes, at specific excitation and detection frequencies. The beatmaps are extracted by first stacking 2D spectra as a function of T, which are then fit to a multiexponential decaying function, to capture the "slow" population dynamics. This fit is subtracted to isolate the amplitude modulations due to vibrational coherences in the time domain. This is repeated for the Re and Im parts of the (absorptive, rephasing or nonrephasing) signal. Re and Im residuals are then

Optics EXPRESS

combined to obtain a complex-valued residuals matrix, which is Fourier transformed [3] over the waiting time T. The beatmaps are obtained by "slicing" the ($\tilde{\nu}_1$, $\tilde{\nu}_T$, $\tilde{\nu}_3$) 3D dataset at $\tilde{\nu}_T$ frequencies (i.e., the Fourier pair of T) corresponding to Raman active modes of interest. The detectability of these modulations is a sensitive function of SNR, as most of the signal intensity has been subtracted, leaving only the noise and the weak oscillations. The results are shown in Fig. 5 for 90 shots per coherence time averaging and in Supplement 1 (Figs. S15-16) for the 45 and 180 shot averaging.

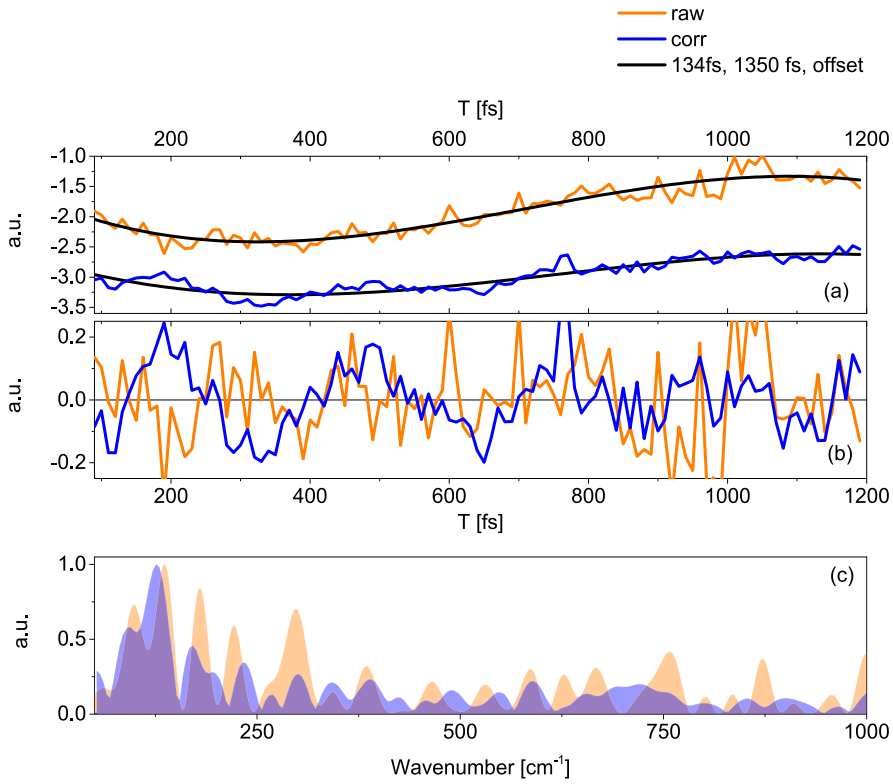

Fig. 5. (a) Rephasing Real HB2DES traces of DAE during T at selected excitation and detection wavenumbers, marked as magenta squares in Fig. 3(b), (c), are shown as solid orange and blue lines, respectively. T is scanned in 10 fs steps. Each coherence time is averaged over 90 laser shots. Solid black lines are fits to the population relaxation dynamics, whose lifetimes are reported in the legend. (b) Residuals of the fits shown in (a). (c) Fourier transforms of the zero-padded residuals shown in (b), whose shaded areas follow the color code of (a), (b).

Waiting time (T) traces from the ESA region of two rephasing real HB2DES measurements on DAE at $\tilde{\nu}_1 = 17068\,\mathrm{cm}^{-1}$, $\tilde{\nu}_3 = 21515\,\mathrm{cm}^{-1}$, (coordinates marked by magenta squares in Fig. 3(b),(c)) acquired with (blue) and without (orange) active noise referencing are reported in Fig. 5(a). Multiexponential fits from the global analysis to the experimental data points are shown as solid black lines. Data are fit to a ~100 fs risetime followed by an incomplete ps decay, in good agreement with literature [66,68]. Fit residuals, shown in Fig. 5(b), show significant differences between the two datasets. Whilst a weak (~10% of the signal amplitude) damped oscillation with ~300 fs period and sub-ps dephasing time dominates the noise-corrected trace (blue), the residuals of the unreferenced 2D data (orange) are dominated by noise. Figure 5(c) shows the Fourier transform over the residuals in 5b. The Fourier spectra (shaded blue and orange) at

Optics EXPRESS

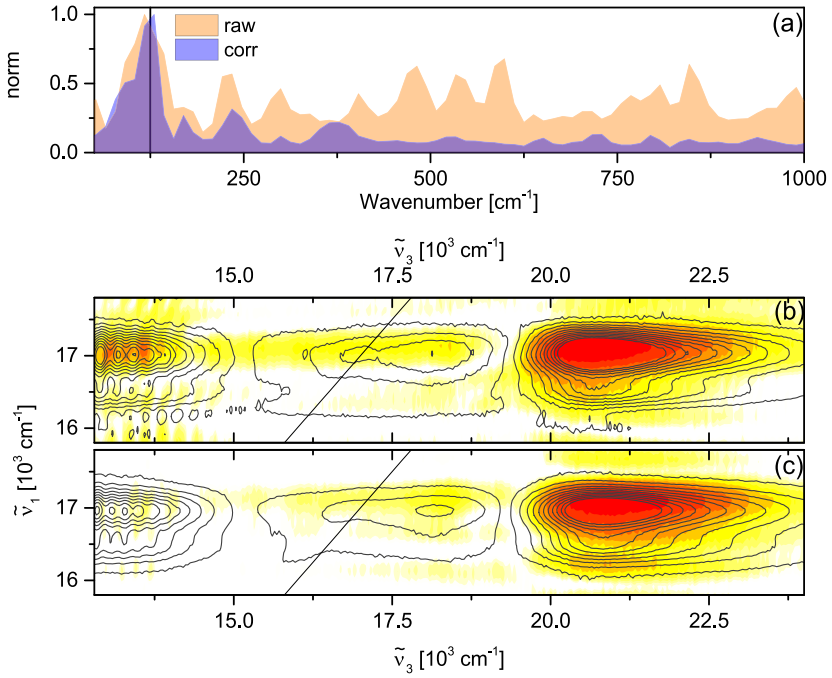

Fig. 6. (a) Rephasing "summary" impulsive Raman spectra of raw (orange) and corrected (blue) DAE data, each coherence time is averaged over 90 shots. (b) Rephasing beatmap of the raw data at +125 cm^{-1} is shown as white-yellow-red heatmap. Contour lines show the real part of the absorptive 2D spectrum at T=300 fs. (c) Same as (b) for the noise corrected data.

these coordinates show a dominating low frequency peak at 125 cm^{-1}, in good agreement with experimental observation of time-resolved Raman and TA by Valley *et al.* and Sotome *et* al. who reported, low frequency, excited state coherent amplitude modulations at 117 cm^{-1} and ca. 140 cm^{-1} after impulsive excitation of DAE and a closely related derivative [66,69]. This low frequency feature is at least a factor of two larger than the background peaks in the noise corrected data (blue), while the raw data (orange) present artefacts whose amplitude is ≥ 50% of the signal. The same effect is evident in the data obtained by averaging 45 laser shots per coherence time (see Supplement 1 Fig. S15), whilst it becomes less significant when the averaging is increased to 180 shots per coherence time (Fig. S16).

The integration of the Fourier transformed residuals over $\tilde{\nu}_1$ and $\tilde{\nu}_3$ yields what is called a summary impulsive Raman spectrum containing contributions from rephasing ground and excited state vibrational coherences, which is used as a guide for the beatmap analysis. These data are reported in Fig. 6(a), again revealing the 125 cm^{-1} peak. As for the single trace case (Fig. 5(c)), the amplitude of the high frequency artefacts is suppressed by a factor of ~2.5 (integral ratio) in the active noise corrected dataset. These summary Raman spectra are a useful guide to the presence of Raman active frequencies [70,71]. Their observation in turn suggests modes which have undergone a significant displacement during optical excitation and may be relevant to the reaction coordinate (e.g., to ring opening in the case of DAE). The observed frequency can be compared with calculations to assign the mode. Clearly the noisier spectrum from the uncorrected data has the potential to lead to misleading assignments, since the noisier data leads to additional modes, and there are many low frequency modes are found in calculation of large

Optics EXPRESS

molecules, such that it is not easy to determine which will be enhanced, especially for excited electronic states [72,73].

Figure 6(b), (c) show the raw and noise corrected rephasing $+125\,\mathrm{cm}^{-1}$ beatmaps, respectively, overlaid with contour lines representing the corresponding real absorptive HB2DES spectra at $T = 300$ fs (reproduced from Fig. 3(b),(c)). In both beatmaps the strongest feature is localized on the blue side of the excitation axis, on the high energy ESA ($\tilde{\nu}_1 = 17000\,\mathrm{cm}^{-1}$ $\tilde{\nu}_3 > 19500\,\mathrm{cm}^{-1}$). Such excitation-detection coordinates are consistent with a rephasing ESA Liouville space pathway [8], i.e., an S_1 vibrational coherence modulating the ESA signal during T, resonantly enhanced by the displacement between the S_1 and S_n potential energy surfaces minima. Finally, the raw beatmap (Fig. 6(b)) also shows amplitude on the low energy side of the probe ($\tilde{\nu}_1 = 17000\,\mathrm{cm}^{-1}$ $\tilde{\nu}_3 = 13000\text{-}15000\,\mathrm{cm}^{-1}$), but the "fringe" pattern, and the absence of such signal in the corrected beatmap (Fig. 6(c)) suggesting that this is an artefact due to fluctuations in the WLC probe, which is successfully removed by the active noise correction. Beatmaps acquired for the different averaging conditions are shown in Supplement 1 Figs. S17-18 and are in agreement with the data presented above.

4. Conclusions

We described a referenced HB2DES method that uses a pair of NOPA pulses, generated by an AOPDF, and a visible continuum probe, in a partially collinear geometry. Dedicated compressors in the pump and probe arms of the experiment yield a flat instrument response function, with time duration < 50 fs. Shot-to-shot cycling of the interpulse relative carrier wave phase and scanning of the coherence time delay, combined with well-established 3×1 phase cycling data processing allowed measurement of Re and Im parts of rephasing, nonrephasing and absorptive half-broadband 2D spectra in <1 min per waiting time. The dual channel referenced detection was based on the active noise reduction algorithm for heterodyned spectroscopies described by Feng *et al.* [45].

The performance of the spectrometer was evaluated by comparing the SNR of coherence time interferograms at selected wavelengths on unreferenced vs noise-corrected referenced data of the photoswitch DAE for different levels of signal averaging. A SNR enhancement factor of ~2, (in addition to the SNR improvement due to averaging) is found. The referencing method was further benchmarked by extracting the weak oscillatory features and the corresponding impulsive Raman spectra and beatmaps, arising from nuclear wavepacket motion in the S_1 state of DAE. A $+125\,\mathrm{cm}^{-1}$ excited state Raman active mode and its rephasing beatmap are reported.

This work shows how active-noise corrected referencing is an effective method of improving the SNR of 2D electronic spectrometers, in addition to previously described enhancements for TA and 2DIR [46,47]. It has been demonstrated that this approach allows collection of acceptable SNR data on systems which generate relatively weak signals (DAE) in a realistic collection time. An extension to the method in which the B-matrix is collected multiple times during the measurement may allow longer collection times. Further, active noise reduction has implications for higher-order ($\chi^{(5)}$) spectroscopies, such as transient-2DES [74] or "degenerate-broadband" 3DES, [75] whose signals are intrinsically weaker.

Funding. Engineering and Physical Sciences Research Council (EP/J009148/1, EP/J021431/1, EP/V00817X/1).

Acknowledgments. We would like to thank Dr. James Bull for providing the DAE sample and Dr. Luca Bolzonello, Dr. Palas Roy, and Dr. Dale Green for helpful discussions.

Disclosures. The authors declare no conflicts of interest.

Data availability. Data underlying the results presented in this paper are not publicly available at this time but may be obtained from the authors upon reasonable request.

Supplemental document. See Supplement 1 for supporting content.

Optics EXPRESS

References

1. P. Hamm and M. Zanni, *Concepts and Methods of 2D Infrared Spectroscopy* (Cambridge University Press, 2011), 1.
2. A. Gelzinis, R. Augulis, V. Butkus, B. Robert, and L. Valkunas, "Two-dimensional spectroscopy for non-specialists," Biochim. Biophys. Acta, Bioenerg. **1860**(4), 271–285 (2019).
3. F. V. d. A. Camargo, L. Grimmelsmann, H. L. Anderson, S. R. Meech, and I. A. Heisler, "Resolving Vibrational from Electronic Coherences in Two-Dimensional Electronic Spectroscopy: The Role of the Laser Spectrum," Phys. Rev. Lett. **118**(3), 033001 (2017).
4. F. D. Fuller, J. Pan, A. Gelzinis, V. Butkus, S. S. Senlik, D. E. Wilcox, C. F. Yocum, L. Valkunas, D. Abramavicius, and J. P. Ogilvie, "Vibronic coherence in oxygenic photosynthesis," Nat. Chem. **6**(8), 706–711 (2014).
5. D. Zigmantas, E. L. Read, T. Mancal, T. Brixner, A. T. Gardiner, R. J. Cogdell, and G. R. Fleming, "Two-dimensional electronic spectroscopy of the B800-B820 light-harvesting complex," Proc. Natl. Acad. Sci. U. S. A. **103**(34), 12672 (2006).
6. G. S. Schlau-Cohen, T. R. Calhoun, N. S. Ginsberg, E. L. Read, M. Ballottari, R. Bassi, R. van Grondelle, and G. R. Fleming, "Pathways of Energy Flow in LHCII from Two-Dimensional Electronic Spectroscopy," J. Phys. Chem. B **113**(46), 15352–15363 (2009).
7. E. Cassette, R. D. Pensack, B. Mahler, and G. D. Scholes, "Room-temperature exciton coherence and dephasing in two-dimensional nanostructures," Nat. Commun. **6**(1), 6086 (2015).
8. G. Bressan, D. Green, Y. Chan, P. C. Bulman Page, G. A. Jones, S. R. Meech, and I. A. Heisler, "One- to Two-Exciton Transitions in Perylene Bisimide Dimer Revealed by Two-Dimensional Electronic Spectroscopy," J. Phys. Chem. A **123**(8), 1594–1601 (2019).
9. A. Halpin, P. J. M. Johnson, R. Tempelaar, R. S. Murphy, J. Knoester, T. L. C. Jansen, and R. J. D. Miller, "Two-dimensional spectroscopy of a molecular dimer unveils the effects of vibronic coupling on exciton coherences," Nat. Chem. **6**(3), 196–201 (2014).
10. G. Bressan, A. N. Cammidge, G. A. Jones, I. A. Heisler, D. Gonzalez-Lucas, S. Remiro-Buenamañana, and S. R. Meech, "Electronic Energy Transfer in a Subphthalocyanine–Zn Porphyrin Dimer Studied by Linear and Nonlinear Ultrafast Spectroscopy," J. Phys. Chem. A **123**(27), 5724–5733 (2019).
11. F. V. A. Camargo, H. L. Anderson, S. R. Meech, and I. A. Heisler, "Time-Resolved Twisting Dynamics in a Porphyrin Dimer Characterized by Two-Dimensional Electronic Spectroscopy," J. Phys. Chem. B **119**(46), 14660–14667 (2015).
12. E. Meneghin, F. Biscaglia, A. Volpato, L. Bolzonello, D. Pedron, E. Frezza, A. Ferrarini, M. Gobbo, and E. Collini, "Biomimetic Nanoarchitectures for Light Harvesting: Self-Assembly of Pyropheophorbide-Peptide Conjugates," J. Phys. Chem. Lett. **11**(19), 7972–7980 (2020).
13. L. Bolzonello, F. Fassioli, and E. Collini, "Correlated Fluctuations and Intraband Dynamics of J-Aggregates Revealed by Combination of 2DES Schemes," J. Phys. Chem. Lett. **7**(24), 4996–5001 (2016).
14. C. Lambert, F. Koch, S. F. Völker, A. Schmiedel, M. Holzapfel, A. Humeniuk, M. I. S. Röhr, R. Mitric, and T. Brixner, "Energy Transfer Between Squaraine Polymer Sections: From Helix to Zigzag and All the Way Back," J. Am. Chem. Soc. **137**(24), 7851–7861 (2015).
15. J. Lim, D. Palecek, F. Caycedo-Soler, C. N. Lincoln, J. Prior, H. Von Berlepsch, S. F. Huelga, M. B. Plenio, D. Zigmantas, and J. Hauer, "Vibronic origin of long-lived coherence in an artificial molecular light harvester," Nat. Commun. **6**, 4–10 (2015).
16. H. Li and S. T. Cundiff, *2D Coherent Spectroscopy of Electronic Transitions*, 1st ed. (Elsevier Inc., 2017).
17. J. Cao, R. J. Cogdell, D. F. Coker, H.-G. Duan, J. Hauer, U. Kleinekathöfer, T. L. C. Jansen, T. Mančal, R. J. D. Miller, J. P. Ogilvie, V. I. Prokhorenko, T. Renger, H.-S. Tan, R. Tempelaar, M. Thorwart, E. Thyrhaug, S. Westenhoff, and D. Zigmantas, "Quantum biology revisited," Sci. Adv. **6**(14), 4888 (2020).
18. D. Finkelstein-Shapiro, P. Mante, S. Sarisozen, L. Wittenbecher, I. Minda, S. Balci, T. Pullerits, and D. Zigmantas, "Understanding radiative transitions and relaxation pathways in plexcitons," Chem **7**(4), 1092–1107 (2021).
19. M. Righetto, L. Bolzonello, A. Volpato, G. Amoruso, A. Panniello, E. Fanizza, M. Striccoli, and E. Collini, "Deciphering hot- and multi-exciton dynamics in core–shell QDs by 2D electronic spectroscopies," Phys. Chem. Chem. Phys. **20**(27), 18176–18183 (2018).
20. M. Kullmann, S. Ruetzel, J. Buback, P. Nuernberger, and T. Brixner, "Reaction Dynamics of a Molecular Switch Unveiled by Coherent Two-Dimensional Electronic Spectroscopy," J. Am. Chem. Soc. **133**(33), 13074–13080 (2011).
21. U. Selig, F. Langhojer, F. Dimler, T. Löhrig, C. Schwarz, B. Gieseking, and T. Brixner, "Inherently phase-stable coherent two-dimensional spectroscopy using only conventional optics," Opt. Lett. **33**(23), 2851 (2008).
22. T. Brixner, T. Mančal, I. V. Stiopkin, and G. R. Fleming, "Phase-stabilized two-dimensional electronic spectroscopy," J. Chem. Phys. **121**(9), 4221–4236 (2004).
23. L. Bolzonello, A. Volpato, E. Meneghin, and E. Collini, "Versatile setup for high-quality rephasing, non-rephasing, and double quantum 2D electronic spectroscopy," J. Opt. Soc. Am. B **34**(6), 1223 (2017).
24. R. Moca, S. R. Meech, and I. A. Heisler, "Two-Dimensional Electronic Spectroscopy of Chlorophyll a: Solvent Dependent Spectral Evolution," J. Phys. Chem. B **119**(27), 8623–8630 (2015).
25. R. Augulis and D. Zigmantas, "Two-dimensional electronic spectroscopy with double modulation lock-in detection: enhancement of sensitivity and noise resistance," Opt. Express **19**(14), 13126 (2011).
26. M. L. Cowan, J. P. Ogilvie, and R. J. D. Miller, "Two-dimensional spectroscopy using diffractive optics based phased-locked photon echoes," Chem. Phys. Lett. **386**(1-3), 184–189 (2004).

Optics EXPRESS

27. J. O. Tollerud and J. A. Davis, "Coherent multi-dimensional spectroscopy: Experimental considerations, direct comparisons and new capabilities," Prog. Quantum Electron. **55**, 1–34 (2017).
28. F. D. Fuller and J. P. Ogilvie, "Experimental implementations of two-dimensional fourier transform electronic spectroscopy," Annu. Rev. Phys. Chem. **66**(1), 667 (2015).
29. Y. Song, A. Schubert, E. Maret, R. K. Burdick, B. D. Dunietz, E. Geva, and J. P. Ogilvie, "Vibronic structure of photosynthetic pigments probed by polarized two-dimensional electronic spectroscopy and ab initio calculations," Chem. Sci. **10**(35), 8143–8153 (2019).
30. N. S. Ginsberg, Y. C. Cheng, and G. R. Fleming, "Two-dimensional electronic spectroscopy of molecular aggregates," Acc. Chem. Res. **42**(9), 1352 (2009).
31. P. Roy, G. Bressan, J. Gretton, A. N. Cammidge, and S. R. Meech, "Ultrafast Excimer Formation and Solvent Controlled Symmetry Breaking Charge Separation in the Excitonically Coupled Subphthalocyanine Dimer," Angew. Chem., Int. Ed. **60**(19), 10568–10572 (2021).
32. V. Sundström, "Femtobiology," Annu. Rev. Phys. Chem. **59**(1), 53–77 (2008).
33. M. Son, S. Mosquera-Vázquez, and G. S. Schlau-Cohen, "Ultrabroadband 2D electronic spectroscopy with high-speed, shot-to-shot detection," Opt. Express **25**(16), 18950 (2017).
34. X. Ma, J. Dostál, and T. Brixner, "Broadband 7-fs diffractive-optic-based 2D electronic spectroscopy using hollow-core fiber compression," Opt. Express **24**(18), 20781 (2016).
35. L. Mewes, R. A. Ingle, A. Al Haddad, and M. Chergui, "Broadband visible two-dimensional spectroscopy of molecular dyes," J. Chem. Phys. **155**(3), 034201 (2021).
36. G. Cerullo, C. Manzoni, L. Lüer, and D. Polli, "Time-resolved methods in biophysics. 4. Broadband pump–probe spectroscopy system with sub-20 fs temporal resolution for the study of energy transfer processes in photosynthesis," Photochem. Photobiol. Sci. **6**(2), 135–144 (2007).
37. U. Megerle, I. Pugliesi, C. Schriever, C. F. Sailer, and E. Riedle, "Sub-50 fs broadband absorption spectroscopy with tunable excitation: putting the analysis of ultrafast molecular dynamics on solid ground," Appl. Phys. B **96**(2-3), 215–231 (2009).
38. G. Bressan, M. Jirasek, P. Roy, H. L. Anderson, S. R. Meech, and I. A. Heisler, "Population and coherence dynamics in large conjugated porphyrin nanorings," Chem. Sci. **13**(33), 9624–9636 (2022).
39. P. F. Tekavec, J. a Myers, K. L. M. Lewis, and J. P. Ogilvie, "Two-dimensional electronic spectroscopy with a continuum probe," Opt. Lett. **34**(9), 1390 (2009).
40. F. D. Fuller, D. E. Wilcox, and J. P. Ogilvie, "Pulse shaping based two-dimensional electronic spectroscopy in a background free geometry," Opt. Express **22**(1), 1018 (2014).
41. S. H. Shim and M. T. Zanni, "How to turn your pump-probe instrument into a multidimensional spectrometer: 2D IR and Vis spectroscopies via pulse shaping," Phys. Chem. Chem. Phys. **11**(5), 748–761 (2009).
42. J. A. Myers, K. L. M. Lewis, P. F. Tekavec, and J. P. Ogilvie, "Two-color two-dimensional Fourier transform electronic spectroscopy with a pulse-shaper," Opt. Express **16**(22), 17420–17428 (2008).
43. H. S. Tan, "Theory and phase-cycling scheme selection principles of collinear phase coherent multi-dimensional optical spectroscopy," J. Chem. Phys. **129**(12), 124501 (2008).
44. Z. Zhang, K. L. Wells, E. W. J. Hyland, and H.-S. Tan, "Phase-cycling schemes for pump–probe beam geometry two-dimensional electronic spectroscopy," Chem. Phys. Lett. **550**, 156–161 (2012).
45. Y. Feng, I. Vinogradov, and N.-H. Ge, "General noise suppression scheme with reference detection in heterodyne nonlinear spectroscopy," Opt. Express **25**(21), 26262 (2017).
46. J. Kübel, S. Westenhoff, and M. Maj, "Giving voice to the weak: Application of active noise reduction in transient infrared spectroscopy," Chem. Phys. Lett. **783**(August), 139059 (2021).
47. K. C. Robben and C. M. Cheatum, "Edge-pixel referencing suppresses correlated baseline noise in heterodyned spectroscopies," J. Chem. Phys. **152**(9), 094201 (2020).
48. C. R. Hall, J. Conyard, I. A. Heisler, G. Jones, J. Frost, W. R. Browne, B. L. Feringa, and S. R. Meech, "Ultrafast Dynamics in Light-Driven Molecular Rotary Motors Probed by Femtosecond Stimulated Raman Spectroscopy," J. Am. Chem. Soc. **139**(21), 7408–7414 (2017).
49. G. Bressan, M. D. Peeks, H. L. Anderson, S. R. Meech, and I. A. Heisler, "Time-Resolved Structural Dynamics of Extended π-Electron Porphyrin Nanoring," J. Phys. Chem. C **123**(44), 27222–27229 (2019).
50. A. Ricci, A. Jullien, N. Forget, V. Crozatier, P. Tournois, and R. Lopez-Martens, "Grism compressor for carrier-envelope phase-stable millijoule-energy chirped pulse amplifier lasers featuring bulk material stretcher," Opt. Lett. **37**(7), 1196 (2012).
51. I. A. Heisler, R. Moca, F. V. A. Camargo, and S. R. Meech, "Two-dimensional electronic spectroscopy based on conventional optics and fast dual chopper data acquisition," Rev. Sci. Instrum. **85**(6), 063103 (2014).
52. J. Réhault, M. Maiuri, A. Oriana, and G. Cerullo, "Two-dimensional electronic spectroscopy with birefringent wedges," Rev. Sci. Instrum. **85**(12), 123107 (2014).
53. W. Zhu, R. Wang, C. Zhang, G. Wang, Y. Liu, W. Zhao, X. Dai, X. Wang, G. Cerullo, S. Cundiff, and M. Xiao, "Broadband two-dimensional electronic spectroscopy in an actively phase stabilized pump-probe configuration," Opt. Express **25**(18), 21115 (2017).
54. N. M. Kearns, R. D. Mehlenbacher, A. C. Jones, and M. T. Zanni, "Broadband 2D electronic spectrometer using white light and pulse shaping: noise and signal evaluation at 1 and 100 kHz," Opt. Express **25**(7), 7869 (2017).

Optics EXPRESS

55. S. Yan and H. S. Tan, "Phase cycling schemes for two-dimensional optical spectroscopy with a pump-probe beam geometry," Chem. Phys. **360**(1-3), 110–115 (2009).
56. N. M. Kearns, A. C. Jones, M. B. Kunz, R. T. Allen, J. T. Flach, and M. T. Zanni, "Two-Dimensional White-Light Spectroscopy Using Supercontinuum from an All-Normal Dispersion Photonic Crystal Fiber Pumped by a 70 MHz Yb Fiber Oscillator," J. Phys. Chem. A **123**(13), 3046–3055 (2019).
57. L. A. Bizimana, J. Brazard, W. P. Carbery, T. Gellen, and D. B. Turner, "Resolving molecular vibronic structure using high-sensitivity two-dimensional electronic spectroscopy," J. Chem. Phys. **143**(16), 164203 (2015).
58. B. Spokoyny, C. J. Koh, and E. Harel, "Stable and high-power few cycle supercontinuum for 2D ultrabroadband electronic spectroscopy," Opt. Lett. **40**(6), 1014 (2015).
59. J. Lu, Y. Lee, and J. M. Anna, "Extracting the Frequency-Dependent Dynamic Stokes Shift from Two-Dimensional Electronic Spectra with Prominent Vibrational Coherences," J. Phys. Chem. B **124**(40), 8857–8867 (2020).
60. D. B. Turner, "Standardized specifications of 2D optical spectrometers," Results Chem. **1**, 100001 (2019).
61. W. P. Carbery, B. Pinto-Pacheco, D. Buccella, and D. B. Turner, "Resolving the Fluorescence Quenching Mechanism of an Oxazine Dye Using Ultrabroadband Two-Dimensional Electronic Spectroscopy," J. Phys. Chem. A acs.jpca. 9b03632 (2019).
62. M. Irie, T. Lifka, S. Kobatake, and N. Kato, "Photochromism of 1,2-Bis(2-methyl-5-phenyl-3-thienyl)perfluorocyclopentene in a Single-Crystalline Phase," J. Am. Chem. Soc. **122**(20), 4871–4876 (2000).
63. S. Shim, T. Joo, S. C. Bae, K. S. Kim, and E. Kim, "Ring Opening Dynamics of a Photochromic Diarylethene Derivative in Solution," J. Phys. Chem. A **107**(40), 8106–8110 (2003).
64. K. Seo, I. Eom, S. Shim, C. H. Kim, and T. Joo, "Ring Closure Reaction Pathway of a Diarylethene in Solution Using Femtosecond Time-resolved Fluorescence Spectra," Bull. Korean Chem. Soc. **40**(4), 352–358 (2019).
65. T. Kim, C. Lin, J. D. Schultz, R. M. Young, and M. R. Wasielewski, "π-Stacking-Dependent Vibronic Couplings Drive Excited-State Dynamics in Perylenediimide Assemblies," J. Am. Chem. Soc. **144**(25), 11386–11396 (2022).
66. H. Sotome, T. Nagasaka, K. Une, S. Morikawa, T. Katayama, S. Kobatake, M. Irie, and H. Miyasaka, "Cycloreversion Reaction of a Diarylethene Derivative at Higher Excited States Attained by Two-Color, Two-Photon Femtosecond Pulsed Excitation," J. Am. Chem. Soc. **139**(47), 17159–17167 (2017).
67. H. Sotome, H. Okajima, T. Nagasaka, Y. Tachii, A. Sakamoto, S. Kobatake, M. Irie, and H. Miyasaka, "Geometrical Evolution and Formation of the Photoproduct in the Cycloreversion Reaction of a Diarylethene Derivative Probed by Vibrational Spectroscopy," ChemPhysChem **21**(14), 1524–1530 (2020).
68. H. Sotome, K. Une, T. Nagasaka, S. Kobatake, M. Irie, and H. Miyasaka, "A dominant factor of the cycloreversion reactivity of diarylethene derivatives as revealed by femtosecond time-resolved absorption spectroscopy," J. Chem. Phys. **152**(3), 034301 (2020).
69. D. T. Valley, D. P. Hoffman, and R. A. Mathies, "Reactive and unreactive pathways in a photochemical ring opening reaction from 2D femtosecond stimulated Raman," Phys. Chem. Chem. Phys. **17**(14), 9231–9240 (2015).
70. T. Brixner, J. Stenger, H. M. Vaswani, M. Cho, R. E. Blankenship, and G. R. Fleming, "Two-dimensional spectroscopy of electronic couplings in photosynthesis," Nature **434**(7033), 625–628 (2005).
71. F. Milota, V. I. Prokhorenko, T. Mancal, H. Von Berlepsch, O. Bixner, H. F. Kauffmann, and J. Hauer, "Vibronic and vibrational coherences in two-dimensional electronic spectra of supramolecular J-aggregates," J. Phys. Chem. A **117**(29), 6007–6014 (2013).
72. D. Green, P. Roy, C. R. Hall, J. N. Iuliano, G. A. Jones, A. Lukacs, P. J. Tonge, and S. R. Meech, "Excited State Resonance Raman of Flavin Mononucleotide: Comparison of Theory and Experiment," J. Phys. Chem. A **125**(28), 6171–6179 (2021).
73. T. J. Quincy, M. S. Barclay, M. Caricato, and C. G. Elles, "Probing Dynamics in Higher-Lying Electronic States with Resonance-Enhanced Femtosecond Stimulated Raman Spectroscopy," J. Phys. Chem. A **122**(42), 8308–8319 (2018).
74. A. Mandal, J. D. Schultz, Y.-L. Wu, A. F. Coleman, R. M. Young, and M. R. Wasielewski, "Transient Two-Dimensional Electronic Spectroscopy: Coherent Dynamics at Arbitrary Times along the Reaction Coordinate," J. Phys. Chem. Lett. **10**(13), 3509–3515 (2019).
75. Z. Zhang, K. L. Wells, M. T. Seidel, and H. S. Tan, "Fifth-order three-dimensional electronic spectroscopy using a pump-probe configuration," J. Phys. Chem. B **117**(49), 15369–15385 (2013).